Friction
https://doi.org/10.1007/s40544-024-0943-y
ISSN 2223-7690
CN 10-1237/TH
RESEARCH ARTICLE

Nano-multilayered ZrN–Ag/Mo–S–N film design for stable anti-frictional performance at a wide range of temperatures

Hongbo JU[1,2,3,†,*], Jing LUAN[2,†], Junhua XU[1], Albano CAVALEIRO[2], Manuel EVARISTO[2], Filipe FERNANDES[2,4]

[1] *School of Materials Science and Engineering, Jiangsu University of Science and Technology, Zhenjiang 212003, China*

[2] *Department of Mechanical Engineering, CEMMPRE, ARISE, University of Coimbra, Rua Luís Reis Santos, Coimbra 3030-788, Portugal*

[3] *TINT - Laboratory for Tribology and Interface Nanotechnology, Faculty of Mechanical Engineering, University of Ljubljana, Aškerčeva 6, Ljubljana 1000, Slovenia*

[4] *CIDEM, ISEP - Polytechnic of Porto, Rua Dr. António Bernardino de Almeida, Porto 4249-015, Portugal*

Received: 06 March 2024 / Revised: 26 April 2024 / Accepted: 29 May 2024

Abstract: A multilayer film, composed by ZrN–Ag (20 nm) and Mo–S–N (10 nm) layers, combining the intrinsic lubricant characteristics of each layer was deposited using DC magnetron sputtering system, to promote lubrication in a wide-range of temperatures. The results showed that the ZrN–Ag/Mo–S–N multilayer film exhibited a sharp interface between the different layers. A face-centered cubic (fcc) dual-phases of ZrN and Ag co-existed in the ZrN–Ag layers, whilst the Mo–S–N layers displayed a mixture of hexagonal close-packed MoS2 (hcp-MoS_2) nano-particles and an amorphous phase. The multilayer film exhibited excellent room temperature (RT) triblogical behavior, as compared to the individual monolayer film, due to the combination of a relative high hardness with the low friction properties of both layers. The reorientation of MoS_2 parallel to the sliding direction also contributed to the enhanced anti-frictional performance at RT. At 400 °C, the reorientation of MoS_2 as well as the formation of MoO_3 phase were responsible for the lubrication, whilst the hard t-ZrO_2 phase promoted abrasion and, consequently, led to increasing wear rate. At 600 °C, the Ag_2MoO_4 double-metal oxide was the responsible for the low friction and wear-resistance; furthermore, the observed transformation from t-ZrO_2 to m-ZrO_2, could also have contributed to the better tribological performance.

Keywords: DC magnetron sputtering; ZrN–Ag/Mo–S–N multilayer film; tribological properties; tribo-phases

1 Introduction

Friction and wear, exhibiting a profound impact on human society due to their influence on energy consumption, can be considered as a bottleneck in the development of key industrial technologies [1, 2]. Traditional lubricants, such as oils and greases, have been widely used to enhance the tribological performance and extend the lifetime of many mechanical components [3]. However, the lubrication performance of the oils at high temperature is significantly reduced, leading to the premature failure of the parts [4]. Thus, industry efforts on research and development, in the last years, are focused on the development of solid self-lubricant coatings. The main objective is to improve both anti-friction and wear-resistance properties, in a wide range of temperatures, to replace the conventional liquid lubrication, that might contain harmful additives [5].

In the literature it is extensively reported that self-lubricant films for high temperature can be achieved by combining the intrinsic properties of hard nitride-based films with low friction elements (e.g. soft metals, fluorides, oxides, etc.) which, by their own properties or by the combination with other elements, can provide low friction properties [6]. For instance,

† Hongbo JU and Jing LUAN contributed equally to this work.

* Corresponding author: Hongbo JU, E-mail: hbju@just.edu.cn

Ag additions to binary ZrN films, using magnetron sputtering, have been shown to improve the tribological properties. The diffusion of silver at elevated temperatures to the wear track significantly drops the friction coefficient and, consequently, the wear rate [7]. Nevertheless, at room and intermediary temperatures the self-lubricant properties of the ZrN–Ag, with relative high hardness values, are not satisfactory due to the absence of enough Ag element on the wear track [8].

Transition metal dichalcogenides (TMD) films are known to exhibit superlubricity properties in vacuum conditions [9]; however, these films wear out easily at moisture and elevated temperature conditions [10]. Therefore, recent works are focused on the improvement of their tribological properties by alloying with metal [11, 12] or nonmetal elements [13]. For example, addition of N to MoS_2 films could increase the hardness and enhance the tribological performance with a significant decrease of the friction and wear rate from room temperature up to 400 °C [14]. Thus, it is reasonable to assume that the combination of self-lubricant TMD alloyed layers with high temperature self-lubricant ones could be the solution to achieve adequate low friction and wear properties in a wide range of temperatures from room temperature (RT) up to 400 °C or higher. Therefore, a multilayer design alternating TMN-Ag (such as ZrN–Ag) and TMD-N (such as Mo-S-N) layers is a potential solution that should be explored. The TMN-Ag layer can provide low friction and wear at high operating temperatures (up to 400 °C), whilst, the latter can ensure adequate tribological properties at low temperatures. Moreover, the deposition parameters of monolayer films of ZrN–Ag, which showed excellent performances, are similar to the ones used for Mo–S–N films [15]. Thus, a multilayer ZrN–Ag/Mo–S–N film with alternating ZrN–Ag and Mo–S–N layers can be deposited using the magnetron sputtering with approximately ideal processing conditions for both layers. The microstructure and the tribological properties from RT to 600 °C are evaluated. The monolayer films, ZrN–Ag and Mo–S–N with similar chemical composition as the layers in the multilayer structure are also deposited for comparison purposes.

2 Experiment details

A ZrN–Ag/Mo–S–N multilayer film was deposited in a semi-industrial DC magnetron sputtering system on (100) silicon wafers and polished AISI 304 stainless steel (SS) for investigating the structure and the tribological behaviors, respectively. For comparison purposes, two monolayer films, ZrN–Ag and Mo–S–N, were deposited with the same conditions as in the multilayer structure. The substrates were cleaned in alcohol and propanol for 15 min and, then, fixed on the substrate holder located at the center of the chamber. The distance from the targets to substrates was set to 80 mm. 3D schematic representation of the deposition chamber is shown in Fig. 1. Detailed deposition parameters of the ZrN–Ag/Mo–S–N

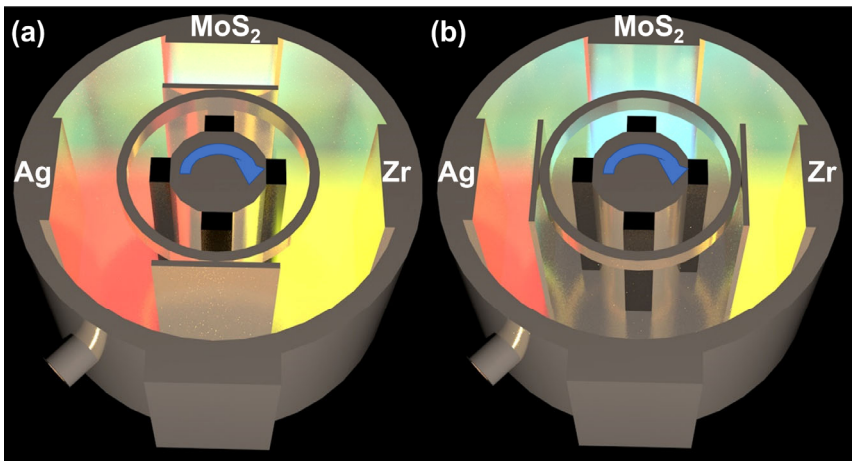

Fig. 1 3D schematic representation of the deposition chamber: (a) shutter rotated to the front of the MoS_2 target to deposit the ZrN–Ag layer, (b) shutter rotated to the front of the Zr and Ag targets to deposit the Mo–S–N layer.

multilayer film by alternating the ZrN–Ag and W–S–N layers are as follows: (i) base pressure of the chamber was below 1×10^{-4} Pa; (ii) a pure Zr layer with a thickness of ~200 nm was deposited under Ar atmosphere (100 sccm corresponding to a deposition pressure of 4×10^{-1} Pa) as an interlayer; (iii) ZrN–Ag layers with a thickness of 20 nm were deposited by applying a power of 2,500 W and 500 W at the Zr and Ag targets, respectively, for 4 min, intercalated with 10 nm thickness Mo–S–N layers deposited by fixing the MoS_2 target power at 700 W for 2 min; (iv) the deposition pressure was set at 5×10^{-2} Pa and the Ar to N_2 ratio was 100:8; (v) no bias and substrate heating were applied during the deposition. The reference ZrN–Ag and Mo–S–N monolayer films were deposited under the same deposition conditions to compare their properties with the multilayer film.

The elemental composition of the monolayer and multilayer films was measured using the electron probe microanalyzer (EPMA, CAMECA SX-50, France) and results showed that the Ag content in ZrN–Ag monolayer film was 2.5 at% and N content in Mo–S–N monolayer film was 29.4 at% N, which is in good agreement with our previous result [16]. The crystal structure of the films was evaluated by X-ray diffractometer (XRD, Shimazu-6000, Japan) with Cu Kα radiation at 40 kV and 35 mA, and 2θ was in the range of 30°–65° with a step of 1°/min. Transmission electron microscopy (TEM, JEOL-2100F, Japan) with an accelerating voltage of 200 kV was used to investigate the cross-sectional microstructure of the multilayer film and to complement the structural analysis of the different layers. A nano-indenter system (CPX + NHT2 + MST, Swiss) using a load of 5 mN for 10 s with an indentation depth below 10% of the films thickness was applied to analyze the films mechanical properties (hardness and elastic modulus). Nine points (3×3) at two different regions were chosen to evaluate the hardness and elastic modulus. The tribological behavior of the films at room temperature, 400, and 600 °C was evaluated using the ball disc wear tribometer (UMT-2, USA) using a counterpart of an alumina ball with a diameter of 9.4 mm. The test was run for 30 min with a circular track of 4 mm diameter at a speed of 50 r/min. The applied load was 3 N. The relative humidity during the room temperature tests was ~30%. The experiment was repeated third to ensure the reproducibility of results. The 3D and its corresponding 2D wear track features were measured using the 3D Profiler (BRUKER, Dektak-XT, Germany), and the wear rate was calculated using the Archard's law.

3 Results and discussion

3.1 Microstructure

Figure 2 illustrates the XRD diffraction pattern of ZrN–Ag/Mo–S–N multilayer film, and the corresponding monolayer films. The monolithic ZrN–Ag film displays seven diffraction peaks. The diffraction peak at ~34° corresponds to the silicon substrate (PDF card #80-0018), three other phases, fcc-ZrN (peaks at ~34°, ~39°, and ~57°, PDF card #89-3839), Zr interlayer (peak at ~35°, PDF card #89-4916), and fcc-Ag (peaks at ~44° and ~63°, PDF card #89-3722), were identified, respectively. Thus, a dual-phase fcc-ZrN and fcc-Ag co-exist in the film. The Mo–S–N monolithic film displays the typical XRD diffraction pattern of sputtered TMD alloyed films, i.e. the peak observed at ~34° (hcp-MoS_2, PDF card #89-2905) is broad and displays an extended shoulder to the right side [17]. This is attributed to the turbostractic stacking of the S–Mo–S layers resulting in a series of plans of type (10L) (L=1, 2, 3) [18]. The addition of nitrogen to MoS_2 led to the formation of an amorphous phase and, thereby, to a weakening and broadening of the diffraction peak of MoS_2, as observed in our previous

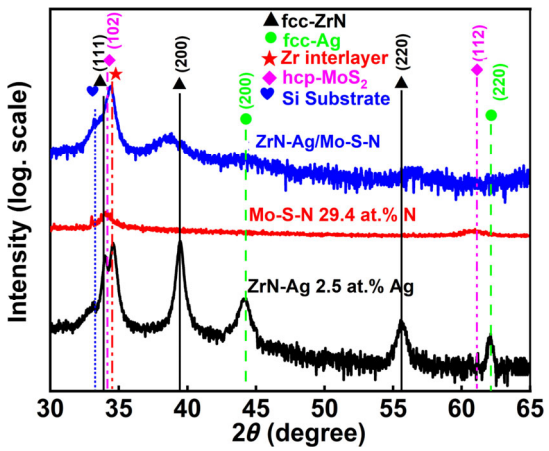

Fig. 2 XRD diffraction patterns of the ZrN–Ag, Mo–S–N monolayer films, and the ZrN–Ag/Mo–S–N multilayer film.

results [19]. As it was expected, the XRD diffraction pattern of the ZrN–Ag/Mo–S–N multilayer film displayed similar phases as the individual ZrN–Ag and Mo–S–N monolayer films. Nevertheless, the Ag signal is almost absent due to the combined effect of (i) low Ag concentration and (ii) very thin ZrN–Ag layer present on the film. No individual and notorious satellite peak is detected. This suggests that the arrangement of the film as a multilayer of Mo–S–N and ZrN–Ag layers does not induce a coherence characteristic, such as the one observed for TiN/AlN [20] and TiN/SiN_x [21].

AFM images of ZrN–Ag, Mo–S–N monolayer films, and ZrN–Ag/Mo–S–N multilayer film are shown in Fig. 3. As shown in Fig. 3(a), the surface morphology of the ZrN–Ag monolayer film exhibits the rolling hills characteristic with a concavoconvex and orderly surface morphology. The roughness of the ZrN–Ag monolayer film is ~1.4 nm. A similar surface morphology is also detected for the Mo–S–N monolayer film, as shown in the Fig. 3(b), but the roughness is ~3.2 nm. Figure 3(c) shows the surface morphology of the ZrN–Ag/Mo–S–N multilayer film, and it still exhibits a rolling hills characteristic with a roughness of ~1.9 nm.

The cross-sectional TEM image of the ZrN–Ag/Mo–S–N multilayer film and its corresponding SEAD patterns are shown in Fig. 4. As shown in Fig. 4(a), the cross-section exhibits a multilayer architecture with well-defined interfaces between the different layers. The alternating bright and dark layers correspond to the Mo–S–N and ZrN–Ag layer, respectively. The modulation period of the multilayer film is ~32.4 nm, with the thickness of the Mo–S–N and ZrN–Ag layers being 11.2 and 21.2 nm respectively. Two different interplanar distance with spacing value of 0.2732 and 0.2368 nm can be observed in the ZrN–Ag layers, corresponding to fcc-ZrN (111) (PDF card #89-3839) and fcc-Ag (111) (PDF card #89-3722) planes. The lattice exhibits a huge number of defects and some amorphous zones can also be detected in this layer. The Mo–S–N layers displayed amorphous character, however, a lattice parameter of 0.2681 nm embed in the amorphous matrix can be observed, corresponding to hcp-MoS_2 (102) plane (PDF card #89-2905). This result is in good agreement with that from the Mo–S–N monolayer film from our previous results [22]. In summary the nano-crystalline phases detected in the multilayer film are fcc-ZrN, fcc-Ag, and hcp-MoS_2.

3.2 Mechanical and tribological properties

The hardness of the monolayer ZrN–Ag and Mo–S–N films are ~22 and ~8 GPa, respectively. The multilayer film displays a hardness value comprised between the hardness of each monolayer films' values (~15 GPa). Although it is well known from the literature that multilayer films can display very high hardness values as compared to their monolayer films, this property is depending on the period thickness of the layers and of the so called superlattice effect [23]. The hardness progressively increases up to a maximum value where the superlattice effect is maximum (differences on the shear moduli of the individual layers materials block the dislocations motion at the layer interfaces causing

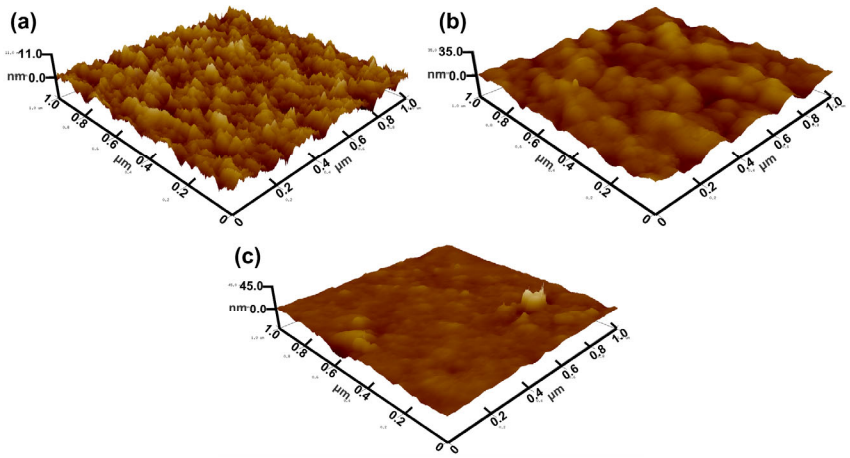

Fig. 3 AFM images of the ZrN–Ag (a), Mo–S–N (b) monolayer films, and the ZrN–Ag/Mo–S–N multilayer film (c).

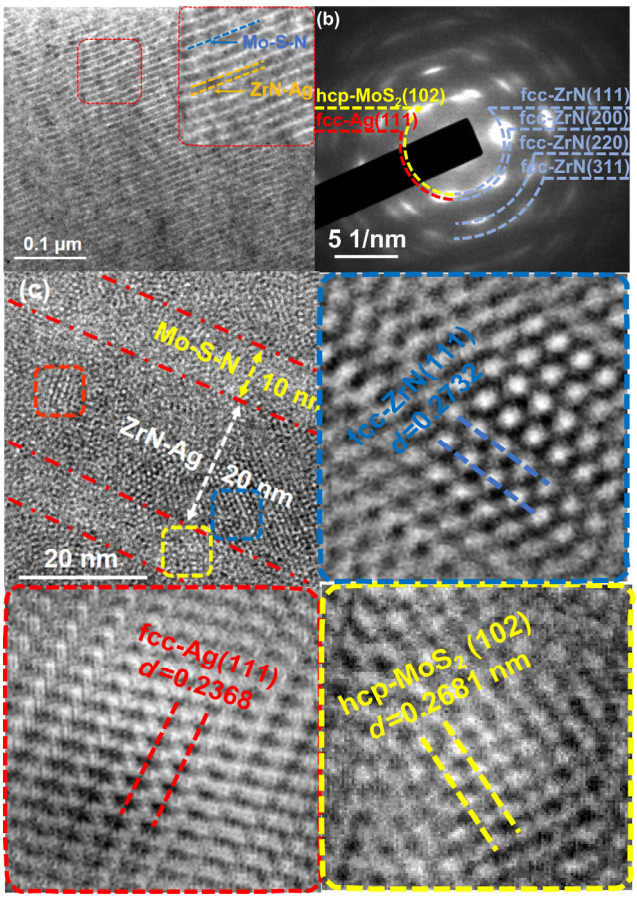

Fig. 4 Cross-sectional of the TEM image of the ZrN–Ag/Mo–S–N multilayer (a), corresponding SAED pattern (b), HRTEM image and the IFFT patterns (c).

periodical strain-stress fields and consequently increasing hardness) and, then, it remains fairly constant, due to the total loss of the superlattice effect. In this case, the multilayers behave as a sum of the individual layers and the hardness of the films is determined by the weighted average of the hardness of the individual layers [24–26]. Therefore, the lower hardness of the multilayer films can be interpreted based on the high period thickness.

The average friction coefficient (COF) and wear rate (WR) of the monolayer and multilayer films for the different testing temperatures are shown in Table 1. At room temperature (RT) COF and WR of the ZrN–Ag monolayer film are ~0.65 and ~4 × 10^{-8} $mm^3/(mm·N)$, respectively, in good agreement with previous work [27]. As expected, the Mo–S–N film displayed a lower friction coefficient but a higher specific wear rate than the ZrN–Ag films' values, which are also identical to the ones reported in the literature [28]. The lower friction coefficient has been attributed to the formation of a low shear tribolayer of MoS_2 with the basal planes parallel to the sliding direction [29, 30]. Despite of the low friction coefficient, this film presents a higher specific wear rate due to the films morphology and structure that makes easier to be removed, due to the exfoliation of the film layer by layer, which are separated by Van der Waals forces, thus easily removed by the shear forces [31]. Besides this, the lower hardness also contributes to the increase of the WR. The multilayer film presents a slight higher COF than the Mo–S–N film, however a significant lower wear rate (by one order of magnitude). Indeed, this film displays the lowest specific wear rate among all the films. At 400 °C similar trend in the COF and WR values is observed, however, as expected, the specific wear rate increases for all the films. The COF value for ZrN–Ag film at this temperature decreased, whilst for the other films increased. At 600 °C the Mo–S–N film fails due to their low oxidation resistance. The ZrN–Ag film shows a COF of 0.4 and an increase of the specific wear rate by two and one order of magnitudes as compared with RT and 400 °C tests respectively. The multilayer film displays a lower friction coefficient than the ZrN–Ag film with a lower specific wear rate by one order of the magnitude in comparison with the

Table 1 Average friction coefficient (COF) and wear rate (WR) of the ZrN–Ag monolayer film, Mo–S–N monolayer film, and ZrN–Ag/Mo–S–N multilayer film for the different testing temperatures.

Film system	RT		400 ℃		600 ℃	
	COF	WR ($mm^3/(mm·N)$)	COF	WR ($mm^3/(mm·N)$)	COF	WR ($mm^3/(mm·N)$)
ZrN–Ag	0.65±0.03	4.0(±0.2)×10^{-8}	0.43±0.02	5.0(±0.2)×10^{-7}	0.4±0.02	1.0(±0.1)×10^{-6}
Mo–S–N	0.20±0.01	3.0(±0.2)×10^{-7}	0.31±0.02	7.0(±0.2)×10^{-7}	\	\
ZrN–Ag/Mo–S–N	0.23±0.01	3.0(±0.2)×10^{-8}	0.36±0.02	8.0(±0.4)×10^{-8}	0.23±0.01	4.0(±0.2)×10^{-7}

ZrN–Ag tested at same temperature. Thus, the combination of the two layers in a multilayer film, allowed to take advantage of the best of the tribological properties of each of the individual ZrN–Ag and Mo–S–N layers. In order to understand the tribological response of the multilayer film as a function of the temperature, detailed analysis of the wear tracks was conducted.

The 3D wear track morphologies of the ZrN–Ag/Mo–S–N multilayer film, tested at various testing temperatures, are shown in Fig. 5. At RT, the wear track surface is smooth and narrow, with exception to a 100 nm depth scratch in the center of the track as shown in Fig. 5(a). During tribological tests, at the initial stage, known as running-in period, the asperities of the film were first in contact with the counterpart, depending on the test conditions and the characteristics of the materials. Then, the asperities are removed and can accumulate in the front of the sliding, being crushed under the load to form a transfer layer on the contact area. However, some of the hard debris incrusted in the transfer layer have sufficient dimension to originate scratch, with deep marks, on the wear track surface, as shown in Fig. 5(a). Increasing the testing temperature to 400 °C the maximum value of COF of the multilayer film is reached. This increase of the friction coefficient can be related with a high number of ploughings sites, resulting in deeper scratches, as suggested by the 3D image in Fig. 5(b). Such a behavior is due to the influence of temperature on decreasing the mechanical properties of the film, giving also rise to the increase of the WR observed as the test temperature increases. The maximum value of the WR is detected at 600 °C in agreement with

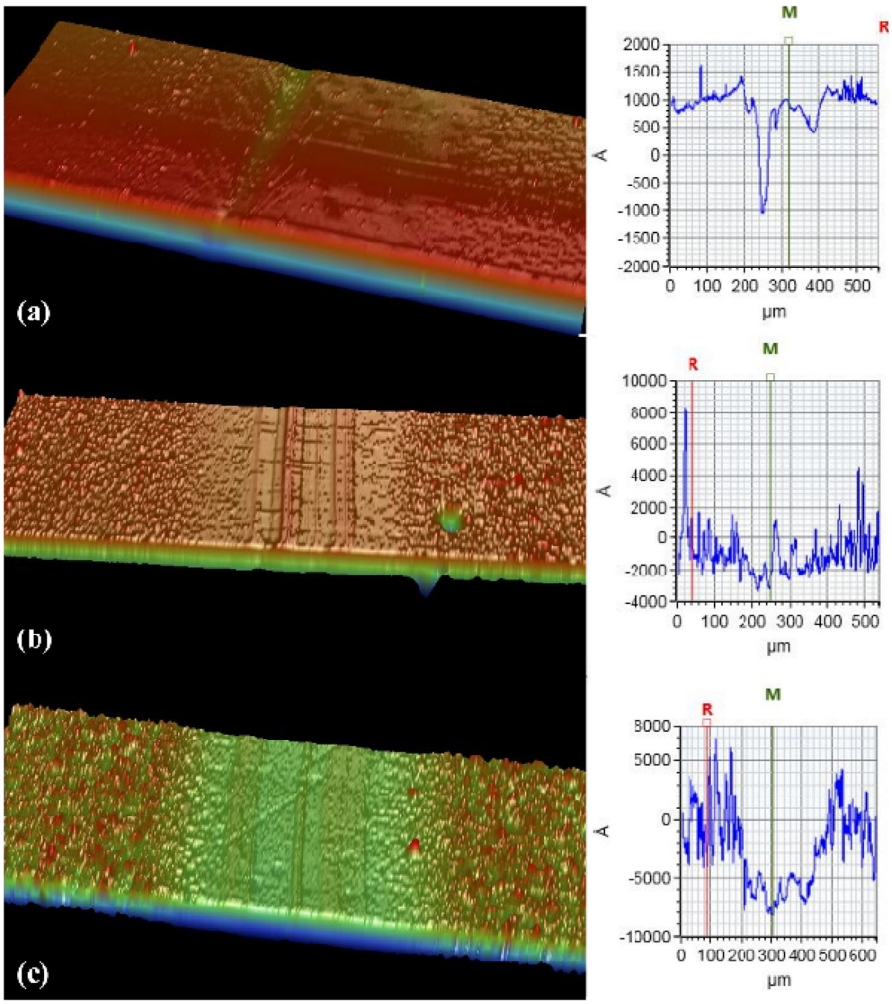

Fig. 5 3D wear track morphologies of the ZrN–Ag/Mo–S–N multilayer film tested at different temperatures: (a) RT, (b) 400 °C, and (c) 600 °C.

the deepest wear track of ~800 nm. Scratches and ploughings exist in the wear surface with a large amounts of debris on both side of the tracks.

The wear debris influencing the wear track morphologies can have different compositions at the different testing temperatures. Raman spectroscopy of the wear track, after the multilayer film is tested at different temperatures, was used to analyze the changes in composition or structure that can occur. Figure 6 shows the spectrum of the as-deposited film for reference with two broad Raman peaks in the spectrum. The spectrum could be divided into a broad peak of low frequency mode ranging 230–360 cm^{-1} and the high frequency mode ranging of 500–600 cm^{-1}. The disorder of single phonons and second order process of the Zr ions contribute to the appearance of the first Raman peak corresponding to the acoustic phonons [32, 33], whilst the phonon bands in the optic range could be determined by the vibrations of the N ions referring to the second peak in the spectrum [34]. Although it is impossible to induce the first-order Raman scattering because of the characterization of inversion symmetry of the fcc phases [35, 36], both the vacancies and amorphization of the ZrN and Ag phases (HRTEM results in Fig. 4(c)) could give rise to Raman phonons [37]. No peaks corresponding to MoS_2 could be indexed in the Raman spectra of the as deposited multilayer film due to its disordered characteristic. The Raman spectrum in the wear track at RT of the multilayer film is similar to the as-deposited one (Fig. 6(b)), with two additional sharp peaks at ~372 and ~410 cm^{-1}, that can be assigned to the E_{2g} and A_{1g} phonon modes of MoS_2 phase, respectively [38, 39]. These signals are attributed to the re-alignment of the MoS_2 hexagonal plans parallel to the sliding direction, at the contact zone. Similar results have been reported for the MoS_2-based monolayer film [40]. At 400 °C the Raman spectrum presents two additional peaks (Fig. 6(c)) at ~151 and ~666 cm^{-1} that can be associated with the formation of tetragonal (t) ZrO_2 [41] and MoO_3 [42]. Although, at elevated temperatures, m-ZrO_2 is more chemical stable than t-ZrO_2, the formation of m-ZrO_2 is more difficult since it needs higher activation energy [43, 44]. The t-ZrO_2 phase, which exhibits an epitaxial structure with the ZrN lattice to reduce the interface energy, firstly forms on the ZrN surface at elevated temperatures [45]. Moreover, the intensity of the peaks belonging to the as-deposited film are weakened when the film is tested at high temperature. Two factors can explain this decrease in intensity: (i) the oxidation of ZrN phases [46] and, thereby, the weakening of the intensity of the ZrN Raman peaks; (ii) the tribo-layer covering the film surface which attenuates the laser spot intensity. At 600 °C the main phases indexed in the Raman spectrum are the monoclinic (m) ZrO_2 (~472 cm^{-1}) [47] and MoO_3 (~205 [48], ~285 [49], and ~666 [50, 51] cm^{-1}), as shown in Fig. 6(d). The right shoulder on the ~666 cm^{-1} peak can be tentatively attributed to Ag_2MoO_4 (~720 cm^{-1}) [52]. The m-ZrO_2 and MoO_3 could be considered as the main tribo-phases based on the Raman peaks intensity, although the existence of Ag_2MoO_4 can also play a significant role in the tribological performance. The evolution of t-ZrO_2 was widely reported in the ZrN based films at elevated temperatures, though m-ZrO_2 exhibits more chemical stability below 1,170 °C. The lower activation energy of ZrN → t-ZrO_2 results in the initial formation of the t-ZrO_2 phase [53, 54]. Moreover, the broaden Raman peak corresponding to as-deposited multilayer is also detected.

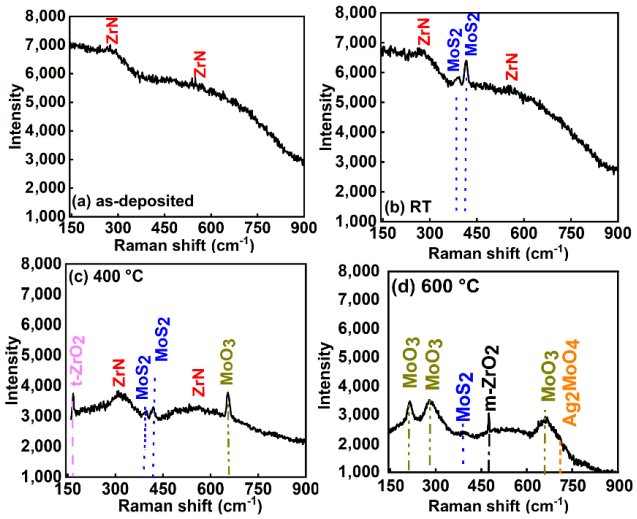

Fig. 6 Raman spectra of the as-deposited ZrN–Ag/Mo–S–N multilayer film (a) and wear track after testing the film at different temperatures: RT (b), 400 °C (c), and 600 °C (d).

As shown in Table 1, globally, the ZrN–Ag/Mo–S–N multilayer film displayed better tribological performance as compared to the ZrN–Ag and Mo–S–N monolayer films. The wear mechanisms of the multilayer film

as a function of testing temperature are sketched in Fig. 7. The explanation for the tribological performance at different testing temperatures can be summarized as follows:

(i) At RT, although a smooth wear track with few deep scratches was formed, Ag and MoS_2 phases in the multilayer film with excellent lubricant nature are the responsible for the low COF. The presence of aligned and well-ordered MoS_2 phase, as detected by Raman, in the contact contributes to the low COF in comparison to the ZrN–Ag film. On the other hand, the relative higher hardness of the multilayer film in comparison to the Mo–S–N one could provide the load-bearing capacity, hindering the easier film wear during experiments, with almost the same low COF. The presence of re-orientated/crystallized MoS_2 crystals on the top surface of the contact provides the low friction, while the protection against hard wear debris comes from the nitride layer.

(ii) At 400 °C, besides the MoS_2 crystallites, a new tribo-phase, MoO_3 and ZrO_2, could be detected in the wear track. Both the MoS_2 phase with the basal planes parallel to the sliding direction, and the lubricant nature of MoO_3 are considered as the main factor to hold the COF in relative low value, compared with ZrN-Ag monolayer film, but the presence of t-ZrO_2 has a detrimental effect on the COF although contributes to ensure the hardness of the wear track surface. However, the hard debris formed during sliding can scratch the track surface and results in the increase of WR.

(iii) At the highest temperature (600 °C), complex synergy actions take place involving both modulation layers, as follows: (a) MoS_2 is not detected anymore which suggests that is oxidized forming MoO_3, known to have a lubricious character; (b) a new double-metal oxide tribo-phase of Ag_2MoO_4 is potentially formed; as shown in the diagram of 4×4 cells, in this phase the –O–Mo–O– is encapsulated by the fragments of –O–Ag–O–, with consequent –Ag–Ag– bonds in the cells; both O–Ag and Ag–Ag allow an easy sliding under the shear force, due to their weak bond energy, providing a lower COF in relation to the Zr–Ag–N layer; (c) the phase transformation of t–ZrO_2 to m–ZrO_2, is accompanied by a volume expansion of ~5%, creating compressive stresses that contributes to the improvement of the anti-wear performance.

4 Conclusions

A new design nano-multilayered ZrN–Ag/Mo–S–N film was deposited using DC magnetron sputtering technology for critical lubrication at elevated temperatures. The microstructure and tribological properties of the multilayer film were investigated and the main conclusions can be summarized as follows:

(1) ZrN–Ag/Mo–S–N multilayer film exhibited a sharp interface between the different layers. A

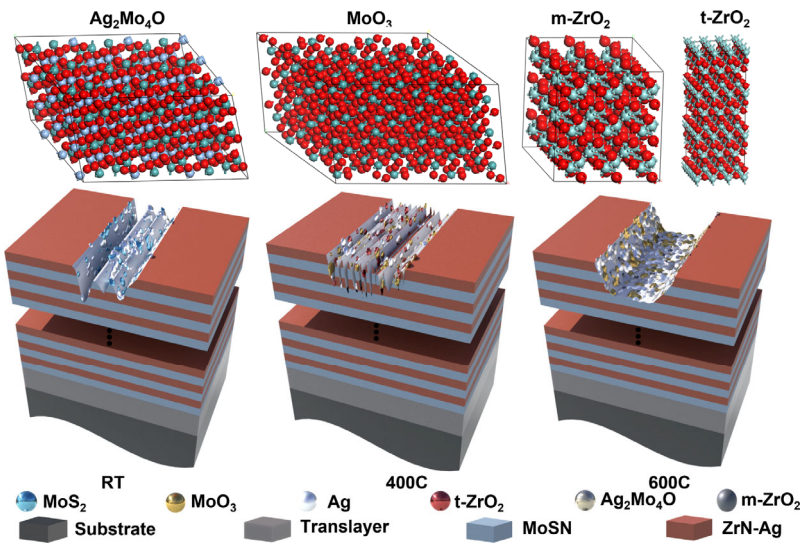

Fig. 7 4×4 supercell 3D representation of Ag_2MoO_4, MoO_3, m-ZrO_2, and t-ZrO_2, and the tribological behavior as a function of testing temperature.

dual-phase of face-centered cubic (fcc) ZrN and fcc-Ag co-existed in the ZrN–Ag layers, whilst, the Mo–S–N layers displayed nano-particle of hcp-MoS_2 inserted in an amorphous matrix.

(2) The multilayer film hardness is ~15 GPa, representing the average values of the hardness of its corresponding modulation layers.

(3) The multilayered ZrN–Ag/Mo–S–N film altering ZrN–Ag and Mo–S–N layers displayed better tribological properties as compared with their corresponding monolayer ones, at the different testing temperatures. At RT the low friction properties of the multilayer film were given by the presence of MoS_2 and Ag phases on the contract. At 400 °C the same phases were determining the low friction, however, the formation of hard t-ZrO_2 led to the increase of the wear rate. At 600 °C new lubricant phases were formed in particular MoO_3 and the double-metal oxide Ag_2MoO_4 on the contract, to result in the low friction. The volume expansion induced by the phase transformation from t-ZrO_2 to m-ZrO_2 contributed to the improvement on the wear rate.

Acknowledgements

This work was supported by the National Natural Science Foundation of China (Nos. 52171071, 51801081, and 52071159), national funds through FCT of Portugal – Fundação para a Ciência e a Tecnologia, under a scientific contract of 2021.04115.CEECIND, and the project of UIDB/00285/2020, LA/0112/2020, MCTool[21] - ref. "POCI-01-0247-FEDER-045940"co-financed via FEDER and FCT-Fundação para a Ciência e a Tecnologia (COMPETE), Outstanding University Young Teachers of "Qing Lan Project" of Jiangsu Province of China, Excellent Talents of "Shenlan Project" of Jiangsu University of Science of China. The authors also thank Fanlin Kong and Yiping Wang for their support to investigate the TEM results.

Declaration of competing interest

The authors have no competing interests to declare that are relevant to the content of this article.

References

[1] Zhao Y C, He Y, Zhang J, Meng C, Zhang X Y, Zhang S L. Effect of high temperature-assisted ultrasonic surface rolling on the friction and wear properties of a plasma sprayed Ni/WC coating on #45 steel substrate. *Surf Coat Technol* **452**: 129049 (2023)

[2] Ju H, Luan J, Wang Y, Bondarev A, Evaristo M, Geng Y, Xu J, Cavaleiro A, Fernandes F. Mutual promotion on the mechanical and tribological properties of the nacre-like self-lubricant film designed for demanding green tribological applications. Friction https://doi.org/10.26599/FRICT.2025.9440963 (2024)

[3] Yang K, Jiang Z T, Chen C, Zhang S H, Liu X. Investigation on the microstructure, tribological performance and corrosion resistance of Ni–Mo coatings deposited by HVOF and APS methods. *Vacuum* **200**: 111023 (2022)

[4] Fang H L, Li Y, Zhang S W, Ding Q, Hu L T. Lubricating performances of oil-miscible trialkylanmmonium carboxylate ionic liquids as additives in PAO at room and low temperatures. *Appl Surf Sci* **568**: 150922 (2021)

[5] Wan L, Cheng M Y, Fu G Y, Wei C, Shi T, Shi S H. Annular laser cladding of $CuPb_{10}Sn10$ copper alloy for high-quality anti-friction coating on 42CrMo steel surface. *Opt Laser Technol* **158**: 108878 (2023)

[6] Torres H, Pichelbauer K, Budnyk S, Schachinger T, Gachot C, Rodríguez Ripoll M. A Ni-Bi self-lubricating Ti_6Al_4V alloy for high temperature sliding contacts. *J Alloys Compd* **944**: 169216 (2023)

[7] Lenzi V, Cavaleiro A, Fernandes F, Marques L. Diffusion of silver in titanium nitride: Insights from density functional theory and molecular dynamics. *Appl Surf Sci* **556**: 149738 (2021)

[8] Ju H B, Yu D, Yu L H, Ding N, Xu J H, Zhang X D, Zheng Y, Yang L, He X C. The influence of Ag contents on the microstructure, mechanical and tribological properties of ZrN-Ag films. *Vacuum* **148**: 54–61 (2018)

[9] Bin Yaqub T, Vuchkov T, Bruyère S, Pierson J F, Cavaleiro A. A revised interpretation of the mechanisms governing low friction tribolayer formation in alloyed-TMD self-lubricating coatings. *Appl Surf Sci* **571**: 151302 (2022)

[10] X. Feng, R. Wang, G. Wei, Y Zheng, H. hu, L. Yang, K. Zhang, H. Zhou. Effect of a micro-textured surface with deposited MoS_2-Ti film on long-term wear performance in vacuum. *Surf Coat Technol* **445**: 128722 (2022)

[11] Torres H, Vuchkov T, Slawik S, Gachot C, Prakash B, Rodríguez Ripoll M. Self-lubricating laser claddings for reducing friction and wear from room temperature to 600 °C. *Wear* **408–409**: 22–33 (2018)

[12] Ju H B, He X C, Yu L H, Xu J H. The microstructure and tribological properties at elevated temperatures of tungsten silicon nitride films. *Surf Coat Technol* **326**: 255–263 (2017)

[13] Rao L X, Liu H, Shao W, Liu H L, Xing X L, Zhou Y F, Shi Z J, Yang Q X. Tailoring the mechanical properties of diamond-like carbon film by doping of trace nonmetal elements: A first-principles study. *J Alloys Compd* **868**: 159151 (2021)

[14] Tiwari P, Jaiswal J, Chandra R. Optical and electrical tunability in vertically aligned MoS_2 thin films prepared by DC sputtering: Role of film thickness. *Vacuum* **198**: 110903 (2022)

[15] Hebbar Kannur K, Huminiuc T, Bin Yaqub T, Polcar T, Pupier C, Héau C, Cavaleiro A. An insight on the MoS_2 tribo-film formation to determine the friction performance of Mo-S-N sputtered coatings. *Surf Coat Technol* **408**: 126791 (2021)

[16] Ju H B, Wang R, Ding N, Yu L H, Xu J H, Ahmed F, Zuo B, Geng Y X. Improvement on the oxidation resistance and tribological properties of molybdenum disulfide film by doping nitrogen. *Mater Des* **186**: 108300 (2020)

[17] Huang J H, Kuo K L, Yu G P. Oxidation behavior and corrosion resistance of vacuum annealed ZrN-coated stainless steel. *Surf Coat Technol* **358**: 308–319 (2019)

[18] Ju H B, Yu L H, Yu D, Asempah I, Xu J H. Microstructure, mechanical and tribological properties of TiN-Ag films deposited by reactive magnetron sputtering. *Vacuum* **141**: 82–88 (2017)

[19] Ju H B, Wang R, Wang W X, Xu J H, Yu L H, Luo H. The microstructure and tribological properties of molybdenum and silicon nitride composite films. *Surf Coat Technol* **401**: 126238 (2020)

[20] Zhou C, Wang J J, Meng J, Li W, Liu P, Zhang K, Ma F C, Ma X, Feng R, Liaw P K. Effects of modulation layer thickness on fracture toughness of a TiN/AlN-Ni multilayer film. *Mater Des* **222**: 111097 (2022)

[21] Sperr M, Zhang Z L, Ivanov Y P, Mayrhofer P H, Bartosik M. Correlating elemental distribution with mechanical properties of TiN/SiNx nanocomposite coatings. *Scr Mater* **170**: 20–23 (2019)

[22] Ju H B, Yu L H, He S, Asempah I, Xu J H, Hou Y. The enhancement of fracture toughness and tribological properties of the titanium nitride films by doping yttrium. *Surf Coat Technol* **321**: 57–63 (2017)

[23] Ma H P, Gu L, Shen Y, Huang W, Liu Y H, Zhu J T, Zhang Q C. Annealing effect on $SiNx/SiO_2$ superlattice with ultrathin sublayer fabricated using plasma-enhanced atomic layer deposition. *Ceram Int* **48**(15): 22123–22130 (2022)

[24] Zhang C, Ouyang S Y, Niu S, Zhao Y, Zhang B S, Feng Y Q, Chen Y. Tuning the mechanical properties of Mo-W alloyed Ni-based multilayered films upon post-annealing at 600 °C via modulation of individual layer thickness. *Vacuum* **207**: 111641 (2023)

[25] Ju H B, Jia P. Microstructure, oxidation resistance and mechanical properties of Nb–Y–N films by reactive magnetron sputtering. *Prot Met Phys Chem Surf* **56**(2): 328–332 (2020)

[26] Ju H B, Jia P, Xu J H, Yu L H, Geng Y X, chen Y H, Liu M H, Wei T Y. The effects of adding aluminum on crystal structure, mechanical, oxidation resistance, friction and wear properties of nanocomposite vanadium nitride hard films by reactive magnetron sputtering. *Mater Chem Phys* **215**: 368–375 (2018)

[27] Baghriche O, Rtimi S, Zertal A, Pulgarin C, Sanjinés R, Kiwi J. Accelerated bacterial reduction on Ag–TaN compared with Ag–ZrN and Ag–TiN surfaces. *Appl Catal B Environ* **174–175**: 376–382 (2015)

[28] Zhang X L, Qiao L, Chai L Q, Xu J, Shi L, Wang P. Structural, mechanical and tribological properties of Mo–S–N solid lubricant films. *Surf Coat Technol* **296**: 185–191 (2016)

[29] Agmon L, Almog R, Gaspar D, Voscoboynik G, Choudhary M, Jopp J, Klausner Z, Ya'akobovitz A, Berkovich R. Nanoscale contact mechanics of the interactions at monolayer MoS_2 interfaces with Au and Si. *Tribol Int* **174**: 107734 (2022)

[30] Ju H B, Yu D, Xu J H, Yu L H, Zuo B, Geng Y X, Huang T, Shao L, Ren L T, Du C Z, et al. Crystal structure and tribological properties of Zr Al Mo N composite films deposited by magnetron sputtering. *Mater Chem Phys* **230**: 347–354 (2019)

[31] Tian R X, Zhao L Y, Wu A M, Zhang S, Zhang G F, Yao M, Huang H. Atomic-level understanding on progressive lithiation of few-layer MoS_2 with surface vacancies. *J Alloys Compd* **939**: 168663 (2023)

[32] Xu S, Hunter N, Zobeiri H, Lin H, Cheng W, Wang X. Distinct optical and acoustic phonon temperatures in nm-thick suspended WS_2: Direct differentiating via acoustic phonon thermal field invariant. *Mater Today Phys* **27**: 100816 (2022)

[33] Ju H B, Ding N, Xu J H, Yu L H, Geng Y X, Ahmed F, Zuo B, Shao L. The influence of crystal structure and the enhancement of mechanical and frictional properties of titanium nitride film by addition of ruthenium. *Appl Surf Sci* **489**: 247–254 (2019)

[34] Priya B, Jasrotia P, Sulania I, Kumar R, Jyoti, Pandey R K, Kumar T. Substrate-dependent fractal growth and wettability of N+ ion implanted V_2O_5 thin films. *Appl Surf Sci* **619**: 156592 (2023)

[35] Tao B R, Qiu R S, Liu Y S, Tan X N, Liu Q. FCC phase transformation of Zr alloy during air cooling and aging. *J Nucl Mater* **551**: 152989 (2021)

[36] Ju H B, Zhou R, Liu S J, Yu L H, Xu J H, Geng Y X. Enhancement of the tribological behavior of self-lubricating nanocomposite Mo2N/Cu films by adding the amorphous SiNx. *Surf Coat Technol* **423**: 127565 (2021)

[37] Cai F, Zhou Q, Chen J K, Zhang S H. Effect of inserting the Zr layers on the tribo-corrosion behavior of Zr/ZrN multilayer coatings on titanium alloys. *Corros Sci* **213**: 111002 (2023)

[38] Mohan M, Shetti N P, Aminabhavi T M. Phase dependent performance of MoS_2 for supercapacitor applications. *J Energy Storage* **58**: 106321 (2023)

[39] Ju H B, Yu D, Xu J H, Yu L H, Geng Y X, Gao T, Yi G, Bian S N. Microstructure, mechanical, and tribological properties of niobium vanadium carbon nitride films. *J Vac Sci Technol A Vac Surf Films* **36**(3): 031511 (2018)

[40] Kim D, Leem J Y. Modified interfaces of ZnO thin films through MoS_2 addition in precursor solution for MoS_2/ZnO heterojunctions and their enhanced ultraviolet photodetection properties. *J Alloys Compd* **905**: 164168 (2022)

[41] Kumaradhas P, Sivapragash M. Comparison of corrosion behaviour of heat treated, ZrO_2 and ZrN PVD coated AZ91D Mg alloy. *Mater Today Proc* **56**: 527–532 (2022)

[42] Ftouhi H, Lamkaouane H, Louarn G, Diani M, Bernède J C, Addou M, Cattin L. Low temperature synthesis of MoS_2 and MoO_3: MoS_2 hybrid thin films via the use of an original hybrid sulfidation technique. *Surf Interfaces* **32**: 102120 (2022)

[43] Liu K X, Pan M F, Zhang Z W, Hong L P, Xie X Q, Yang J Y, Wang S, Wang Z J, Song Y, Wang S. Electrochemical sensor applying ZrO_2/nitrogen-doped three-dimensional porous carbon nanocomposite for efficient detection of ultra-trace Hg^{2+} ions. *Anal Chim Acta* **1231**: 340392 (2022)

[44] Ju H B, He S, Yu L H, Asempah I, Xu J H. The improvement of oxidation resistance, mechanical and tribological properties of W_2 N films by doping silicon. *Surf Coat Technol* **317**: 158–165 (2017)

[45] Alin M, Kozlovskiy A L, Zdorovets M V, Uglov V V. Study of the mechanisms of the t-ZrO_2 → c-ZrO_2 type polymorphic transformations in ceramics as a result of irradiation with heavy Xe^{22+} ions. *Solid State Sci* **123**: 106791 (2022)

[46] Dong M P, Zhu Y B, Li J L. Effect of amorphous phases induced by friction on wear resistance for TaN/ZrN coatings in thermal oxygen environment. *Mater Charact* **198**: 112745 (2023)

[47] Frank F, Tkadletz M, Saringer C, Czettl C, Pohler M, Burghammer M, Todt J, Zalesak J, Keckes J, Schalk N. Investigation of the microstructure of a graded ZrN/$Ti_{0.33}Al_{0.67}$N multilayer coating using cross-sectional characterization methods. *Surf Coat Technol* **453**: 129126 (2023)

[48] Selvakumar G, Palanivel C. A study on synthesis, characterization and catalytic applications of MoO_3-ZnO nanocompositematerial. *Mater Sci Energy Technol* **5**: 36–44 (2022)

[49] Wang Y W, Yang Y, Li H, Ren X X, Wang X Y, Tian W. Reaction and growth mechanisms of MoO_3-Al system in plasma spraying. *J Alloys Compd* **938**: 168661 (2023)

[50] Rani V, Malhotra M, Patial S, Sharma S, Singh P, Khan A A P, Thakur S, Raizada P, Ahamad T, Asiri A M. Formulation strategies for the photocatalytic H_2 evolution and photodegradation using MoO_3-based Z-scheme photocatalysts. *Mater Chem Phys* **299**: 127454 (2023)

[51] Ju H B, Xu J H. Microstructure and tribological properties of NbN-Ag composite films by reactive magnetron sputtering. *Appl Surf Sci* **355**: 878–883 (2015)

[52] Anjum Moinuddin A, Vijay Kotkondawar A, Hippargi G, Anshul A, Rayalu S. Morphologically and hierarchically controlled Ag/Ag_2MoO_4 microspheres for photocatalytic hydrogen generation. *Appl Surf Sci* **597**: 153554 (2022)

[53] Silva J P B, Istrate M C, Hellenbrand M, Jan A, Becker M T, Symonowicz J, Figueiras F G, Lenzi V, Hill M O, Ghica C, et al. Ferroelectricity and negative piezoelectric coefficient in orthorhombic phase pure ZrO_2 thin films. *Appl Mater Today* **30**: 101708 (2023)

[54] Ju H B, Xu J H. Microstructure, oxidation resistance, mechanical and tribological properties of Ti–Y–N films by reactive magnetron sputtering. *Surf Coat Technol* **283**: 311–317 (2015)

Hongbo JU. He is a professor of Jiangsu University of Science and Technology and Marie-Curie-Research-Fellow from MSCA COFUND SCHEME project of Mobility GT. His research interest includes: thin solid films (PVD), super-hard nitride coatings, self-lubrication, and wear resistance coatings suitable for high temperature applications. He published more than 100 papers in the international peer-review journals.

Jing LUAN. She is a Ph.D. student of University of Coimbra. Her research pursuits encompass various facets, notably thin solid coatings (PVD), super-hard nitride coatings, oxidation resistance, self-lubrication, and wear resistance coatings tailored for high-temperature applications.